International Journal of Multiphase Flow 36 (2010) 303–313

Contents lists available at ScienceDirect

International Journal of Multiphase Flow

journal homepage: www.elsevier.com/locate/ijmulflow

The effect of pipe diameter on the structure of gas/liquid flow in vertical pipes

R. Kaji, B.J. Azzopardi *

Faculty of Engineering, University of Nottingham, University Park, Nottingham NG7 2RD, United Kingdom

ARTICLE INFO

Article history:
Received 1 February 2009
Received in revised form 18 November 2009
Accepted 29 November 2009
Available online 4 December 2009

Keywords:
Pipe diameter
Vertical
Flow structure
Air–water

ABSTRACT

Experimental work on two-phase vertical upward flow was carried out using a 19 mm internal diameter, 7 m long pipe and studying the time series of cross-sectional average void fractions and pressure gradient which were obtained simultaneously. With the aid of a bank of published data in which the pipe diameter is the range from 0.5 to 70 mm, the effect of pipe diameter on flow characteristics of two-phase flow is investigated from various aspects. Particularly, the work focuses on the periodic structures of two-phase flow. Average film thicknesses and the gas flow rate where slug/churn and churn/annular flow transitions occur all increase as the diameter of the pipe becomes larger. On the other hand, the pressure gradients, the frequencies of the periodic structures and the velocities of disturbance waves decrease. The velocity of disturbance waves has been used to test the model of Pearce (1979). It is found that the suggested value of Pearce coefficient 0.8 is reasonable for lower liquid flow rates but becomes insufficient for higher liquid flow rates.

1. Introduction

For application in a number of industries, from compact heat exchangers to large diameter deep-water risers in hydrocarbon production, extension of the current knowledge on gas/liquid flows in a wider range of pipe diameters is necessary. Especially in gas/oil industry, with the increase of oil demand and major discoveries of hydrocarbon fields becoming rarer in the conventional offshore, (water depth up to 500 m) the deeper water exploration is emerging. Risers employed for deep water are normally operated under friction dominated conditions. To minimise pressure losses they tend to be of diameters larger than those for which research data is available. However, it has been recognised that gas/liquid flow in such larger diameter pipes is different from that in smaller ones. For example, in such large diameter pipes (approximately >100 mm), it has been reported that the conventional Taylor bubble does not appear, Ohnuki and Akimoto (2000) and Omebere-Iyari (2006).

Although there are applications over a wide range of pipe diameters, few publications have reported systematically on the effect of pipe diameter on two-phase flow structures. Sekoguchi et al. (1985, 1992) and Ide et al. (1993) studied the effect of pipe diameter for annular flow using data taken from pipes of diameter from 0.5 mm to 26 mm. They investigated several parameters such as film thickness, the velocities/frequencies of what they termed liquid lumps, wave length and wave amplitude. For capillary tubes, Ide et al. found that the liquid lump velocity increases with decreasing pipe diameter but decreases suddenly at a pipe diameter of 2 mm for a constant liquid flow rate. They linked this with the change of wave structure having shorter wavelength and lower amplitude in pipes of diameter $\leqslant$1.5–2 mm. Recent investigations by Jayanti et al. (1996) and Vijayan et al. (2001) shows that there is a definite effect of pipe diameter on the conditions at which flooding occurs. They examined pipes of 25, 67 and 99 mm diameter and proposed three mechanisms of flooding condition depending on the pipe diameter: one due to wave transportation for the smallest diameter pipes and the others linked to the transport of entrained droplets or churn-like motion of liquid film for larger ones.

This paper describes the effect of pipe diameter on parameters indicating flow structure by combining the results of time series of cross-sectionally averaged void fraction and pressure gradient from experimental work using a 19 mm internal diameter pipe and a data bank from 5 to 70 mm internal diameter pipes gathered from published work. Focus is on periodic structures in the slug, churn and annular flow patterns.

2. Flow pattern specific model for annular flow

Published models for predicting film thickness and the velocity of disturbance waves are applied to experimental results in the present work for the purpose of their validation. In a number of empirical equations the film thicknesses are correlated with liquid film Reynolds number as in the following example:

$$\delta_l^+ = A\,\mathrm{Re}_{lf}^B, \tag{1}$$

where A and B are constants,

* Corresponding author. Tel.: +44 (0)115 951 4160; fax: +44 (0)115 951 4115.
E-mail address: barry.azzopardi@nottingham.ac.uk (B.J. Azzopardi).

0301-9322/$ - see front matter © 2010 Published by Elsevier Ltd.
doi:10.1016/j.ijmultiphaseflow.2009.11.010

$$\mathrm{Re}_{lf} = \frac{\dot{m}_{lf} D_t}{\eta_l} \quad \text{and} \tag{2}$$

$$\delta_l^+ = \frac{\delta \rho_l}{\eta_l} \sqrt{\frac{\tau_i}{\rho_l}}. \tag{3}$$

Here $\dot{m}_{lf}$ is liquid film mass flux, D_t is pipe diameter, ρ_l is liquid density, η_l is liquid dynamic viscosity, δ is film thickness and τ_i is interfacial shear stress.

Interfacial shear stress in Eq. (3) is given by:

$$\tau_i = \frac{1}{2} f_i \rho_g u_{gs}^2, \tag{4}$$

where f_i is interfacial friction factor, ρ_g is gas density and u_g is gas velocity, respectively.

Ambrosini et al. (1991) reported that the correlations of Asali et al. (1985) and Kosky (1971) agree well with experimental results for lower and higher liquid film Reynolds number, respectively. The transition between these correlations is at $\mathrm{Re}_{lf} = 1000$. The constants A, B in Eq. (1) for correlations of Asali et al. and Kosky are $A = 0.34$; $B = 0.6$ and $A = 0.0512$; $B = 0.875$, respectively.

Interfacial friction factor in Eq. (4) is given by the following equations proposed by Ambrosini et al. (1991) and Holt et al. (1999) depending on gas mass flux, $\dot{m}_g$:

$$\frac{f_i}{f_s} = 1 + 13.8 We_D^{0.2} \mathrm{Re}_g^{-0.6} \left(\delta_g^+ - 200 \sqrt{\frac{\rho_g}{\rho_l}} \right) \quad \text{for } \dot{m}_g \leqslant 100 \text{ kg/m}^2 \text{ s}, \tag{5}$$

$$\frac{f_i}{f_s} = 1 + 13.8 We_D^{0.175} \mathrm{Re}_g^{-0.7} \delta_g^+ \quad \text{for } \dot{m}_g > 100 \text{ kg/m}^2\text{s}, \tag{6}$$

where

$$\mathrm{Re}_g = \frac{\rho_g u_g D_t}{\eta_g}, \tag{7}$$

$$\mathrm{We}_D = \frac{\rho_g u_g^2 D_t}{\sigma}, \tag{8}$$

$$\delta_g^+ = \frac{\delta \rho_g}{\eta_g} \sqrt{\frac{\tau_i}{\rho_g}} \quad \text{and} \tag{9}$$

$$f_s = 0.046 \mathrm{Re}_g^{-0.2}. \tag{10}$$

Here η_g, σ and f_s are liquid dynamic viscosity, surface tension and single phase friction factor, respectively.

For annular flow, the liquid film mass flux in Eq. (2), $\dot{m}_{lf}$, can be derived from mass balance between deposition rate, D, and entrainment rate, E, given by the following differential equation:

$$\frac{d\dot{m}_{lf}}{dz} = \frac{4}{D_t}(D - E), \tag{11}$$

where z is axial distance along the pipe.

The correlations of these parameters proposed by Hewitt and Govan (1990) are applied. Deposition rate is defined based on the particle diffusivity, i.e.,

$$D = kC, \tag{12}$$

where k is the mass transfer coefficient and C is the droplet concentration given by:

$$C = \frac{\dot{m}_e}{\frac{\dot{m}_g}{\rho_g} + \frac{\dot{m}_e}{\rho_l}}. \tag{13}$$

Here $\dot{m}_e$ and $\dot{m}_g$ are entrained and gas mass flux, respectively.

Mass transfer coefficient is correlated with the droplet concentration by:

$$k \sqrt{\frac{\rho_g D_t}{\sigma}} = 0.18 \quad \text{for } \frac{C}{\rho_g} \leqslant 0.3, \tag{14}$$

$$k \sqrt{\frac{\rho_g D_t}{\sigma}} = 0.083 \left(\frac{C}{\rho_g} \right)^{-0.65} \quad \text{for } \frac{C}{\rho_g} > 0.3. \tag{15}$$

Entrainment rate, E, in Eq. (11) can be predicted by:

$$\frac{E}{\dot{m}_g} = 5.75 \times 10^{-5} \left[(\dot{m}_{lf} - \dot{m}_{lfC})^2 \frac{D_t \rho_l}{\sigma \rho_g^2} \right]^{0.316}, \tag{16}$$

where $\dot{m}_{lfc}$ is the critical liquid mass flux on inception of entrainment given by:

$$\dot{m}_{lfc} = \frac{\eta_l}{D_t} \exp \left(5.8504 + 0.4249 \frac{\eta_g}{\eta_l} \sqrt{\frac{\rho_l}{\rho_g}} \right). \tag{17}$$

For disturbance wave velocity the model of Pearce (1979) is applied. This is a generic model applied to both vertical and horizontal flow by Pearce. It is developed from the assumption that the change in momentum in the liquid film is the same as that in vapour core within the section between wave trough and peak and can be expressed as:

$$u_w = \frac{K u_{lf} + u_{gs} \sqrt{\rho_g / \rho_l}}{K + \sqrt{\rho_g / \rho_l}}, \tag{18}$$

where u_{gs} is gas superficial velocity and K is the Pearce coefficient defined by:

$$K = \bar{\delta} / \sqrt{\delta_p \delta_b}, \tag{19}$$

where $\bar{\delta}$, δ_p and δ_b are the average film thickness, peak and base height of the wave, respectively. Pearce suggested that $K = 0.8$ from the experimental data from both horizontal and vertical pipe of 31.8 mm diameter.

The liquid film velocity, u_{lf} (in Eq. (18)), can be calculated from the following equation:

$$u_{lf} = \frac{D_t \dot{m}_{lf}}{4 \rho_l \bar{\delta}}. \tag{20}$$

3. Experimental facility

A schematic diagram of the experimental facility is shown in Fig. 1. This facility is of a 'Double Closed Loop' configuration, in which both gas and liquid are recirculated. The facility consists of a liquid ring compressor unit, a centrifugal pump, a heat exchanger, two cyclones, two measuring tanks, a buffer tank and a separator tank. The test section, made of transparent acrylic resin, has an internal diameter of 19 mm and is 6.87 m tall. In the test section, eight ring-type conductance probes were installed at different axial positions (dimensionless axial distances from mixer were 2, 110, 218, 221, 292, 295, 297 and 300 pipe diameters). In addition, a differential pressure cell is mounted between tappings at 4.24 and 5.53 m from the mixer. The mixing section at the bottom of the test section consisted of a section of pipe wall with 80 holes with 2 mm diameter spaced equally in 8 columns over a length of 50 mm. The liquid was introduced into an annular chamber surrounding this section of pipe.

Air was pumped by the compressor into the buffer tank, whilst water was introduced by the pump via heat exchanger. The air and water were mixed at the bottom of the test section and travelled

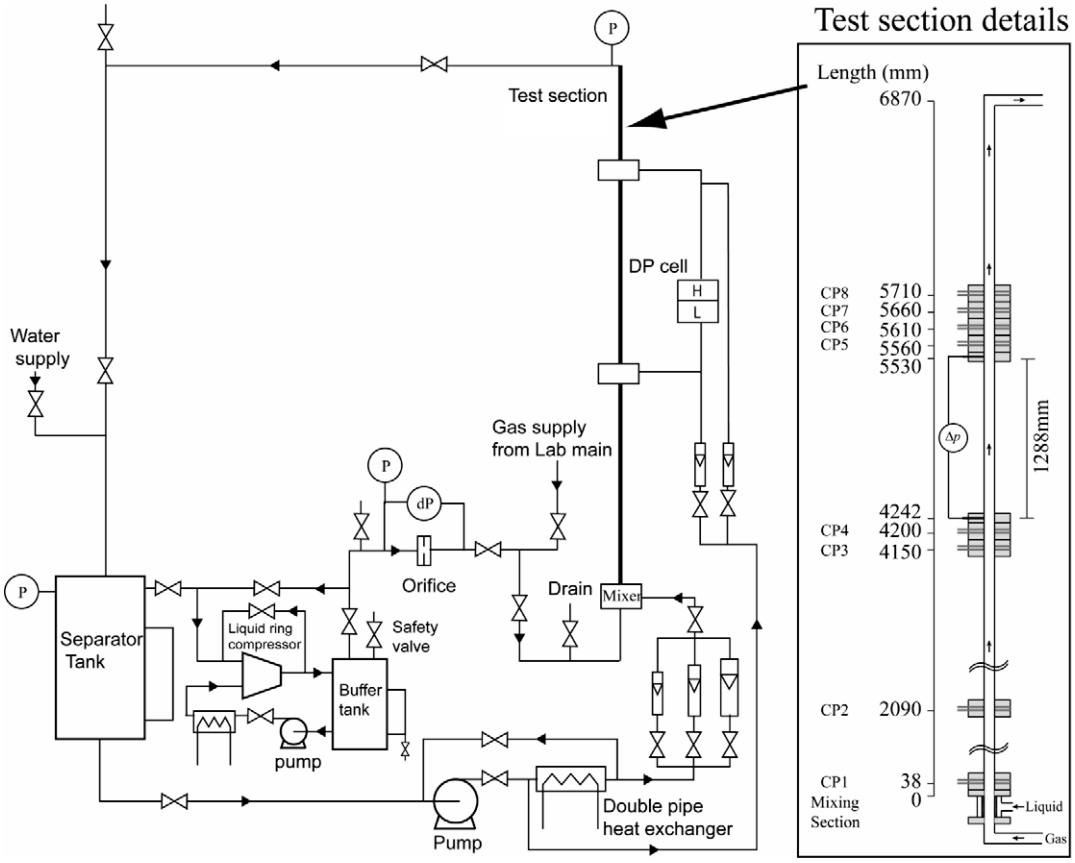

Fig. 1. Experimental facility of 19 mm pipe: Flow sheet and Test section.

upwards. Beyond the test section, the two-phase mixture flowed round a bend, travelled 0.14 m horizontally, and was directed downwards by another bend that led to the separator tank where air and water were separated and returned to the compressor and pump, respectively. The air flow rate was metered by an orifice plate and the water flow rate was determined from one of a bank of calibrated variable area meters. The orifice plate was calibrated using a diaphragm gas meter whilst the variable area meters were by weighing mass of water collected over a fixed time. From these calibrations, the uncertainties of air and water flow rate are ±5% and ±7%, respectively. During the experiment the inlet and outlet liquid temperatures were monitored using two *T*-type thermocouples which were located just before the mixing point and after the test section.

Measurements of void fraction were made by using ring-type conductance probes developed by Fossa (1998). The sensor was constructed by mounting two stainless steel plates between a set of acrylic blocks and machining a hole through them so that they were flush with pipe inner wall. The configuration is characterised by the thickness of electrodes, s, and the distance between them, D_e. The dimensions D_e/D_t and s/D_t were 0.357 and 0.075, respectively. The conductance probe was provided with 20 kHz, −1 to 1 volt peak to peak alternating current, supplied to the Wheatstone bridge diagonally. An instrumentation amplifier, a full wave rectifier and a band pass filter were installed before the signal was sent to the data acquisition board. Known pitfalls for this type of probe were: the liquid conductivity varies with temperature and probe response depends on the cross-sectional phase distribution as well as fraction of liquid. The former problem was solved by keeping the temperature constant during the experiment, whilst the latter was tackled by extensive and careful calibration. The calibration was carried out by inserting plastic cylinders (of diameters between 6 and 18.5 mm) and strings of beads (3 or 6 mm diameter) or packed beds of beads to simulate the gas phase. These represent the annular and dispersed phase structures, respectively. The void fraction was calculated by knowing the diameter of the cylinders and the diameter and concentration of the beads. In addition, a calibration using air bubbles was carried out. From these calibration experiments, the dimensionless conductance, G_e^*, which is defined by dividing the impedance with full water by that when a two-phase mixture is present, can be plotted against actual void fraction as shown in Fig. 2. As expected, the relationships for annular and

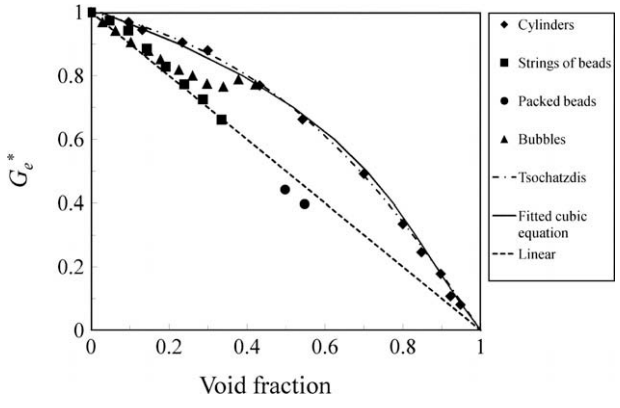

Fig. 2. Calibration curve for conductance probe. G_e^* is the conductance for the pipe full of water divided by two-phase conductance. Cylinders and beads inserted to create void fractions.

bubbly geometries seem to be distinctly different. For annular geometry, the results are well predicted by the theoretical solution of Tsochatzidis et al. (1992), whilst for the bubbly geometry when the bubble voids were modelled by beads, results are distributed around the 45° line. For the different diameters, D_b, of beads examined there is very little effect observed. In some tests a true bubbly flow with zero liquid flow rate was used. The void fraction was determined from the swell of the two-phase mixture above the liquid-only height. These results were similar to those obtained with beads. However, at void fractions >0.2 the data started deviating from the 45° line towards the annular calibration line. This is probably due to the radial concentration of bubble being non-uniform – gas is concentrated in the middle of the pipe. The results presented here were obtained with the calibration curve for annular geometry since most data are taken in the high void fraction region. In the work on void fraction in liquid slugs, the calibration curve for bubble geometry was applied. The uncertainty of the film thickness of annular flow of film thickness <1.5 mm is ±10%.

Together with void fraction measurement, the pressure difference between a pair of tappings 1288 mm apart was measured by a differential pressure cell [Kent Taylor Smart Deltapi K series]. To ensure that there is only one phase in the tapping lines a liquid purging technique was used. This prevented bubbles from entering to the tapping lines. Before the measurement a high purging rate was applied to clear any bubbles from the lines. It was then reduced to an optimum flow rate which is low enough that the measured pressure gradient is not affected by the purge flow. The range of the differential pressure cell is 0–70 kPa of which the resolution is ±45 Pa.

4. Results

Measurements were made of void fraction and pressure drop for gas superficial velocities of 1–33 m/s and liquid superficial velocities 0.03–0.65 m/s.

4.1. Effect of axial distance on void fraction

Axial variation of average void fraction is shown in Fig. 3. Different trends are observed between low and high liquid flow rates, particularly at the boundary gas superficial velocity of 7 m/s. In lower gas flow rate conditions, for low liquid flow rates, void fraction increases asymptotically along the pipe, whilst for high liquid flow rates void fraction decreases with axial distance up to about 100 pipe diameter then increases asymptotically. In higher gas flow rate conditions, for all liquid flow rates, void fraction decreases with axial distance up to about 100 pipe diameters then increases asymptotically. This low void fraction at the entrance might be due to entrainment of the liquid phase. Systematic decrease of void fraction is observed when the liquid flow rate increases. The trend that void fraction decreases with axial distance close to the inlet agree with the results by Wolf et al. (2001), but the present results show more gradual increase than his data. From the figures, it is considered that fully developed flow is achieved at a position between 200 and 300 D_t from the inlet.

4.2. Time series data

Examples of the time series of void fraction and pressure gradient obtained are shown in Fig. 4. The numbers besides the graphs correspond to the Conductance Probes CP1 to CP8 in Fig. 1. The top graph shows the variation of total pressure gradient. The conditions at which these were taken correspond to churn flow. The data was recorded at a frequency of 2.5 kHz for 26 s and show flow development from the bottom to the top of the test pipe. From this figure, it is seen that the number of waves decreases dramatically between the first and second probe. Beyond that the wave structure remains fairly consistent.

4.3. Average void fraction and pressure gradient

The results plotted against gas superficial velocity, for different liquid flow rates, are shown in Fig. 5. In this part data from the upper-most probe was used. The average void fraction increases monotonically with the gas superficial velocity and increases with the liquid superficial velocity. Fig. 6 shows the total pressure gradient against gas superficial velocity. The total pressure gradient shows maxima and minima for lower liquid flow rates, but the trend disappears for high liquid flow rates (liquid superficial velocity >0.25 m/s) where the pressure gradient increases monotonically.

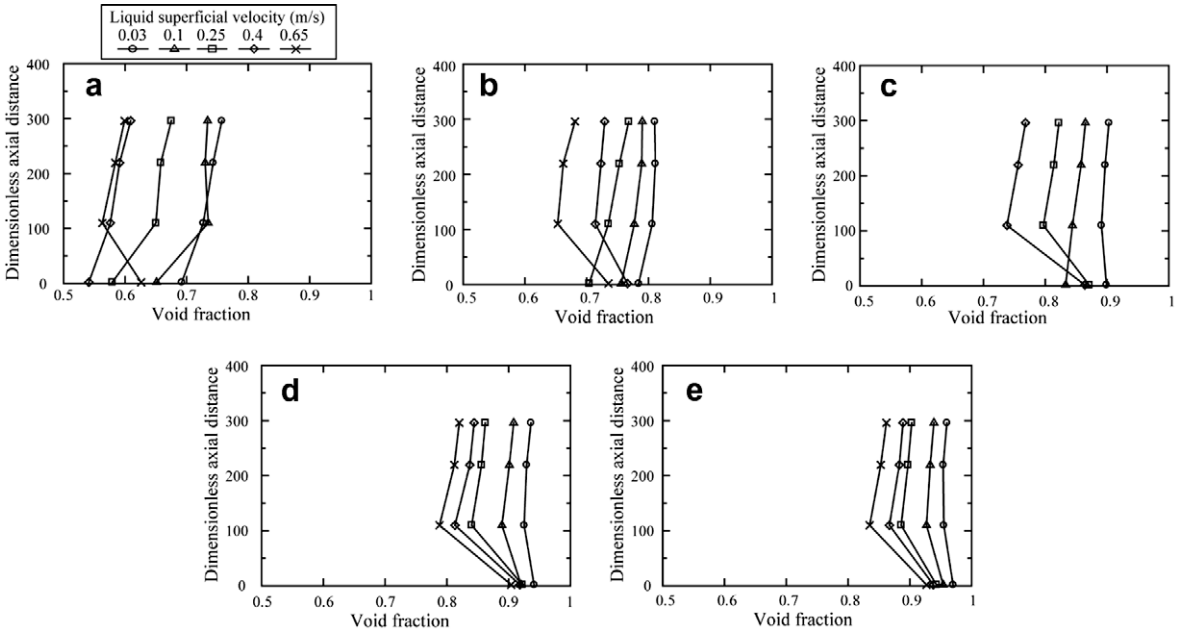

Fig. 3. Examination of flow development using average void fraction (gas superficial velocity: (a) 1 m/s, (b) 3 m/s, (c) 7 m/s, (d) 12 m/s and (e) 24 m/s).

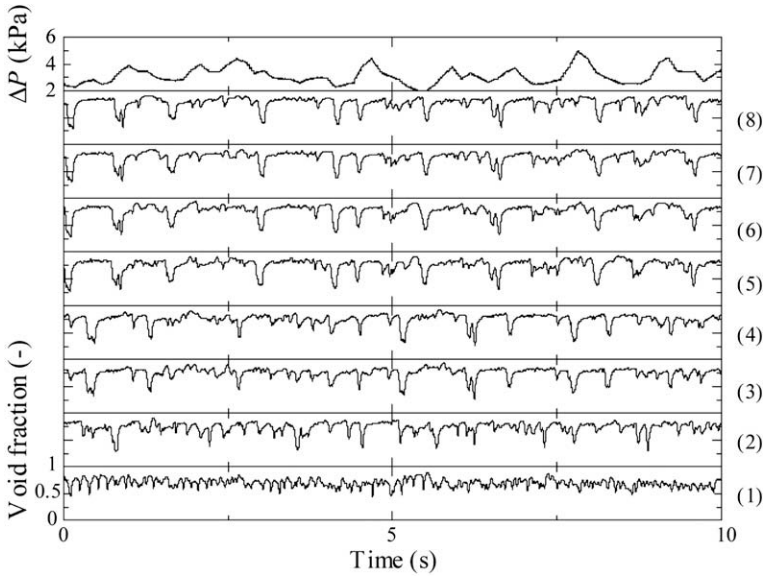

Fig. 4. An example of time series data for the liquid superficial velocity of 0.25 m/s: the gas superficial velocity of 3.0 m/s.

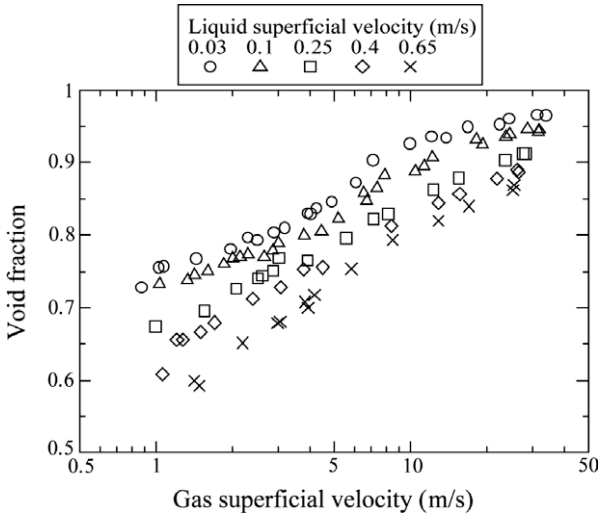

Fig. 5. Variation of void fraction with gas flow rates for different liquid flow rates.

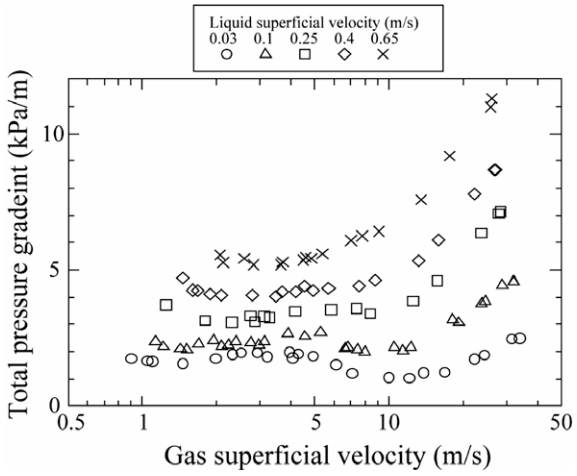

Fig. 6. Variation of total pressure gradient with gas flow rates for different liquid flow rates.

4.4. Base and peak film thicknesses

Information about the mean film thickness as well as the base film in between the disturbance waves and the mean peak film thickness in the annular flow region can be obtained from the time series such as those illustrated in Fig. 4. The film thickness is obtained from the void fraction by the simple geometric relationship:

$$\delta = \frac{D_t}{2}\left(1 - \sqrt{\varepsilon_g}\right). \tag{21}$$

Probability Density Function (PDF) information can be obtained from these times series. Two cases are illustrated in Fig. 7. The lower flow rate one clearly shows two distinct peaks. That at the higher flow rates is less clear. However, it is possible to fit two Gaussian distributions to the data. These are taken to be related to the base film and to the wave peaks. It might be expected that the sum of the Gaussians would give a good fit to the PDF. Whilst this is correct at higher flow rates, there is a lack of agreement between data and the combined Gaussian curve at the lower flow rates as illustrated in Fig. 7. The poor agreement between the peaks might be due to the presence of waves intermediate between the ripples on the base film and the disturbance waves. It was observed that the width of the distributions increased with increasing liquid superficial velocity for both the lower and higher peaks. There was an effect of gas superficial velocity but this became smaller at higher gas velocities. Whilst the increase with liquid superficial velocity was smooth for the lower peak, there was a jump in values for the higher peak at a liquid superficial velocity between 0.1 and 0.25 m/s. The peaks of these Gaussians were used to determine the average values of base and peak thicknesses. These are plotted in Fig. 8 for the range of gas and liquid flow rates studied. Both base and peak values increased with increasing liquid superficial velocity. Increasing gas superficial velocity resulted in a decrease in the thicknesses. Also shown are the mean film thicknesses obtained for each time series. The error bars corresponding to the 10% quoted above are also show. It is clear that it is possible to distinguish between base and peak values with this uncertainty level. The data has been used to determine the value to the dimensionless group $\overline{\delta}/\sqrt{\delta_p\delta_b}$ used by Pearce in the modelling of disturbance wave velocity. The values of the group was found to be 1 ± 0.04 over

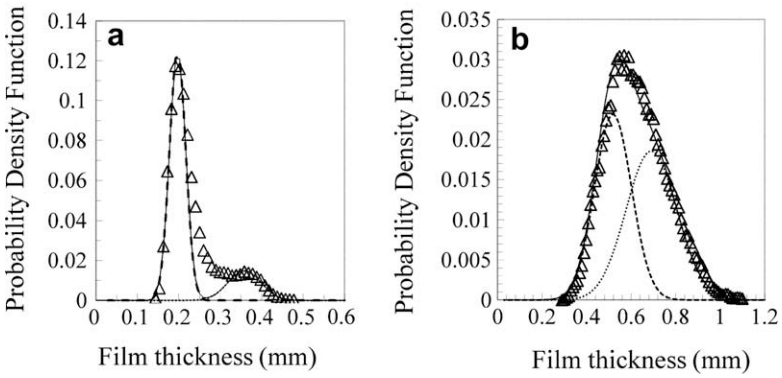

Fig. 7. Probability Density Function of film thickness time series (a) – gas superficial velocity = 15 m/s, liquid superficial velocity = 0.03 m/s; (b) – gas superficial velocity = 30 m/s, liquid superficial velocity = 0.65 m/s. Solid line – summation; dashed line base film distribution; dotted line wave peak distribution.

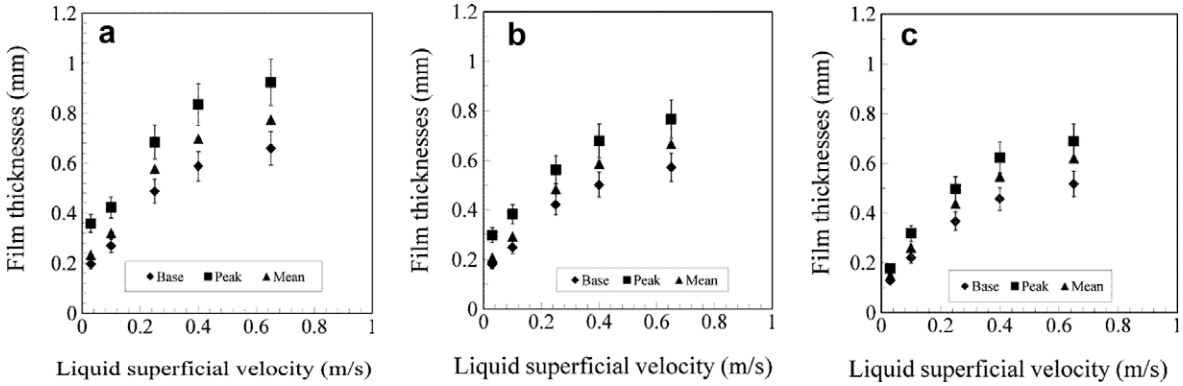

Fig. 8. Effect of liquid superficial velocity on mean, base and peak thicknesses. Gas superficial velocities: (a) 15 m/s, (b) 22 m/s and (c) 30 m/s.

most of the ranges of gas and liquid flow rates studies except at the lowest liquid flow rates where the values dropped down to 0.88.

4.5. Structure velocity

The velocities of the periodic structures, such as bubble concentration waves, slugs, huge waves and disturbance waves, can be obtained by the cross correlation of the signals from two successive probes which are a short distance apart. These are plotted against the mixture velocity, the sum of the gas and liquid superficial velocities, as shown in Fig. 9. At a constant liquid superficial velocity, the loci of structure velocity have maxima and minima. The solid curve shown on the figure is the correlation proposed by Nicklin et al. (1962) for Taylor bubble velocities in slug flow. The experimental values of structure velocity are well correlated by this equation up to the maximum value, although there is a small but systematic deviation as the maximum structure velocity is approached. The initiation of deviation from Nicklin equation shifts to higher gas flow rates with increasing liquid flow rates. Observations as well as examination of the Probability Density Function plots (how often each value of void fraction occurs) show that the data with the positive slope with gas velocity are from slug flow, that with the negative slope are churn flow and the second positive slope are annular flow.

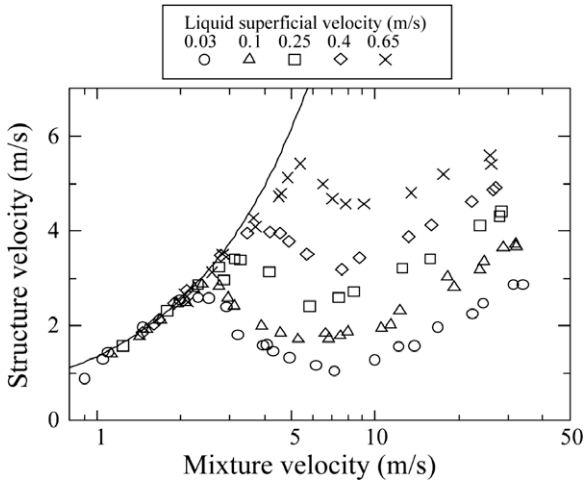

Fig. 9. Periodic structure velocity against mixture velocity for different liquid flow rates (line shows correlation of Nicklin et al. (1962)).

5. The effect of pipe diameter

The data from various pipe diameters have been gathered from sources listed in Table 1. Investigation was focused on the structure of slug and annular flow from the limitation of data bank. The data from much larger pipe diameter, for instance 127 mm employed by Omebere-Iyari (2006), have not been included at this stage since no slug flow was observed. It what follows the data is presented in terms of superficial velocities as the physical properties which appear in dimensionless groups have not been varied. Indeed the data from the sources in Table 1 are all for air and water at room temperature (20–25 °C) so that the viscosity only varies by ±5% from 1 mPa s.

5.1. Direct comparison with time series data

Comparison of the time series of void fraction at the same condition from different pipe diameters (Cases 1, 16, 19 denoted

Table 1
Data bank of various diameter pipes in vertical upflow.

Case	Source	Pipe diameter (mm)	Pressure (bara)	Distance to the sensor (times Dt)	Parameter measured*	Flow pattern	Range of ugs (m/s)	Range of uls (m/s)
1	Omebere-Iyari and Azzopardi (2007)	5	1, 2	400	VF, V	Slug, churn, annlar	0.06–50	0.03–0.65
2	Ide et al. (1993)	0.5	2	360	VF, V	Annular	10–30	0.1–0.5
		0.9		511				
		1.45		352				
		2		325				
		4		513				
		6		342				
3	Jong and Gabriel (2003)	9.5	1	111	VF, V			
4	Martin (1983)	10	1.5	300	VF, DP, V	Annular	22.2–44.4	0.04–0.1
		32	1.5	94			11.1–55.5	0.04–0.08
		58	1.5	52			11.1–33.3	0.02–0.06
5	Tomida and Okazaki (1974)	10	1.05	170	VF, V		2–63	0.128–0.91
6	Willets (1987)	10	1.5	270	VF, DP, V	Annular	10.9–65	0.02–0.14
7	Schadel (1988)	25	1.16	1952	VF, V	Annular	32–116	0.018–0.1
		42	1.28	1162	VF, V		19.5–71.8	0.015–0.067
8	Sekoguchi et al. (1973)	25	1.1	160	VF, V	Annular	15–60	0.013–0.196
9	Sekoguchi and Mori (1997)	25.8	2	207	VF, V	Slug, churn, annular	2–40	0.1–3
10	Ohba and Nagae (1993)	29	1	148	VF, V	Annular	14–31	0.0063–0.038
11	Azzopardi (1986)	32	1.5	156	VF, DP, V	Annular	17.6–44	0.016–0.16
12	Wolf et al. (2001)	32	1.5	325	VF, DP, V	Annular	28.4–95.4	0.01–0.12
13	Belt et al. (2009)	50	1	130	VF, DP, V	Annular	22–42	0.005–0.08
14	Holt (1996)	10	1.5	180	VF, DP, V	Slug, churn, annular	3.6–67	0.04–0.14
15	Sawai et al. (2004)	25.8	1	116	VF, DP, V	Slug, churn, annular	0.55–21.25	0.002–0.4
16	Hernandez Perez and Azzopardi (2006)	38	1	158	VF, DP, V	Bubble, slug, churn	0.18–12.53	0.04–0.73
17	Kaji et al. (2009)	51.2	1	59	VF	Bubble, slug, churn	0.002–0.534	0.004–4.05
		52.3	1	151			0.002–18.97	0.04–4.05
18	Kaji (2008)	70	1	95	VF, V	Bubble, slug, churn	0.02–9.68	0.25–0.65
19	Present	19	1.5	2, 110, 218, 221, 292, 295,297, 300	VF, DP, V	Slug, churn, annular	0.87–33.9	0.03–0.65

* VF: time series void fraction, DP: pressure gradient, V: structure velocity.

in Table 1) is shown in Fig. 10. The combination of gas and liquid superficial velocities considered are 5.5 and 1 m/s, respectively. The *y*-axis scales are the same for all three sources. However, the zeros are systematically offset. It is clear that the frequency of waves decreases with increasing pipe diameter.

5.2. Average film thickness

The average void fraction obtained is plotted against gas superficial velocity, for different pipe diameters (Cases 1, 7, 12, 13, 14, 15, 19), and shown in Fig. 11. This displays data at a constant liquid superficial velocity of 0.1 m/s which have been extracted for illustrative purposes. For those data the system pressure varied from atmospheric to 0.15 MPa. The data from Belt et al. (2009) for 50 mm and Schadel (1988) for 42 mm were not taken at such high liquid flow rates; therefore the information for their cases was obtained by extrapolation using the regression curve derived from plots of film thickness against liquid superficial velocities and converting to void fraction. Whilst there might be a slight difference in the system pressure between the experiments from different pipe diameters, the void fraction shows little effect of pipe diameter. Examination of the variation of film thickness and its interrelation with other parameters has been carried out. Some insight is gained from the simple plot of film thickness non-dimensionalised by pipe diameter against inverse gas superficial velocity, Fig. 12. Here, the data shows two distinct trends. Firstly, in the annular flow region there is little deviation from the main trend for data of pipe diameters. This can be explained in two ways: (i) there was not much effect of pipe diameter on void fraction and film thickness and void fraction are linked by the geometric relationship given by Eq. (21); (ii) examination of the relationship for film thickness shown in Eqs. (1)–(10) shows that the power to which the pipe diameter and the gas superficial velocity would be raised are both about 1. Secondly, in the slug flow region, the film thickness appears to have a much lower dependence on gas superficial velocity though some on pipe diameter. In this region the behaviour of the film (i.e., that surrounding the Taylor bubble) is taken as driven primarily by gravity. The effect of pipe diameter on average film thickness for constant gas superficial velocities of 20, 30, 40 and 50 m/s is shown in Fig. 13. Results were interpolated by using Fig. 11 to obtain the values for these gas superficial velocities. In the figure, the data from Sekoguchi et al. (1985) are also presented. Although slight differences can be seen for small diameter pipes, trends similar to those of Sekoguchi et al. (1985) are clearly seen. The lines are the film thickness obtained from the correlations of Asali et al. (1985) and Kosky (1971) utilising the model of Hewitt and Govan

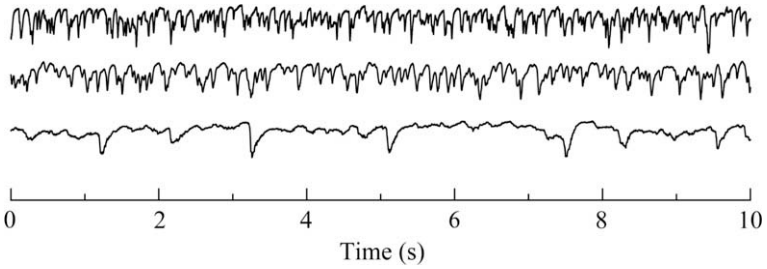

Fig. 10. Time series void fraction from various diameter pipes at the same inlet condition (pipe diameter = top: 5 mm, middle: 19 mm, bottom: 38 mm).

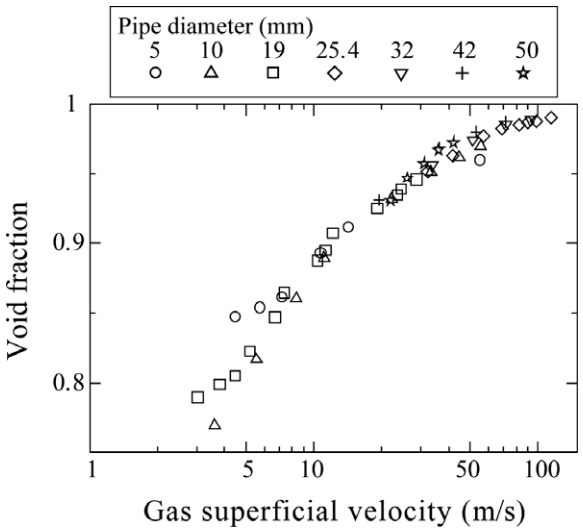

Fig. 11. Average void fraction against gas superficial velocity from various pipe diameters (liquid superficial velocity = 0.1 m/s).

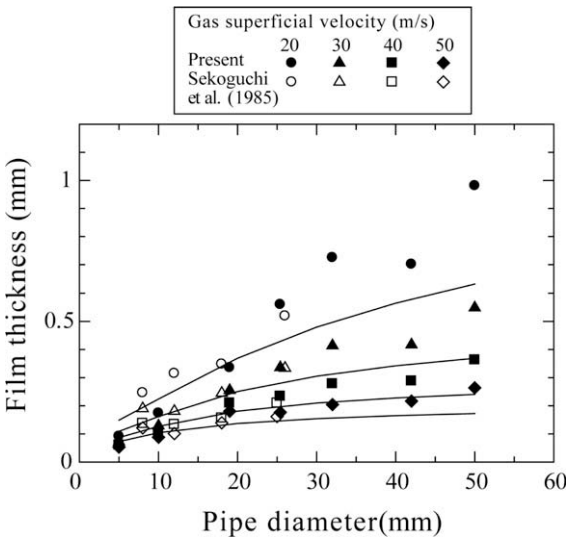

Fig. 13. Effect of pipe diameter of average film thickness and comparison with predictions of correlations of Asali et al. (1985) and Kosky (1971).

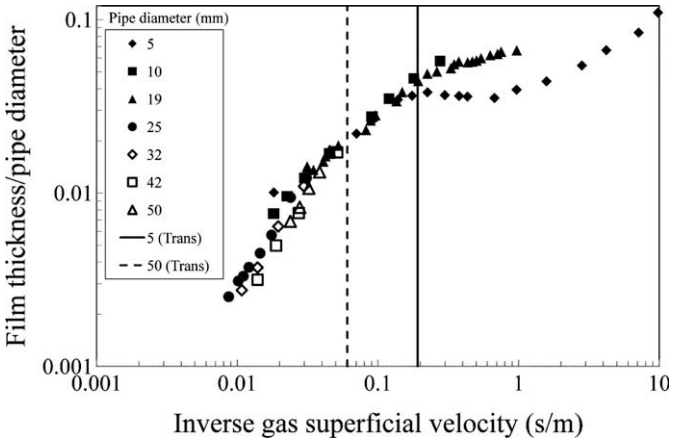

Fig. 12. Relationship between dimensionless film thickness and inverse gas superficial velocity – liquid superficial velocity = 0.1 m/s.

(1990) to provide values of the liquid film flow rates. In all cases a distance from the inlet of 300 pipe diameters (considered as fully developed flow) and atmospheric pressure were used in the calculations. From the figure the model gives lower film thickness than experimental results and the discrepancies increase systematically for larger pipe diameters. This is because that the model underestimates the liquid film flow rate which is caused by underestimation of the deposition rate or overestimation of the entrainment rate for larger pipe diameter. The deviation between experimental results and the model varies from −30% to 40% for 10 to 50 mm diameter pipes. The best prediction is obtained for a 20 mm pipe.

5.3. Pressure gradient

Total pressure gradients from the different pipe diameters (Cases 13–16, 19) have been plotted against gas superficial velocity in Fig. 14. The pressure gradient decreases systematically with increasing pipe diameter. The minimum occurring for each pipe diameter, which is one of the indicators of churn to annular flow transition, shifts to higher gas flow rates with increasing pipe diameter. This indicates that a higher gas flow rate is necessary to cause the transition to annular flow with increasing pipe diameter. Fig. 15 shows the effect of pipe diameters on the frictional pressure gradient. The data from the 19 mm pipe are represented as 20 mm and the 25.8 and 32 mm pipes as 30 mm. The results were compared with the model of Ambrosini et al. (1991) calculated at atmospheric pressure. From the figure, it has been shown that the differences between the correlation and experimental results become bigger with decrease of pipe diameter and with higher gas flow rates. However, the deviations are similar for the whole range of pipe diameters, i.e., −5% to 40% except at the lowest gas flow rates at the largest pipe, where error is −120%. The best prediction obtained is for a 30 mm pipe.

5.4. Structure velocity and flow patterns

Structure velocities from different pipe diameters (Cases 1, 15, 16, 18, 19) were plotted against gas superficial velocity as illustrated in Fig. 16. The curves for the values predicted from the equation of Nicklin et al. (1962) are plotted for the two extreme pipe diameters and show that there is little effect of pipe diameter in those predictions. All the data in the range of this study fit in this

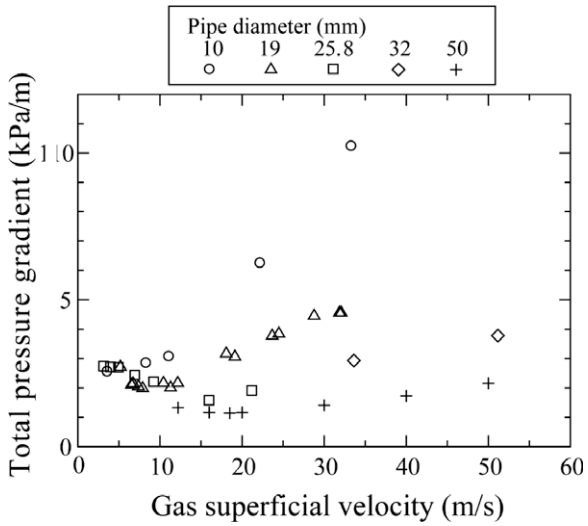

Fig. 14. Total pressure gradient versus gas superficial velocity (liquid superficial velocity = 0.1 m/s).

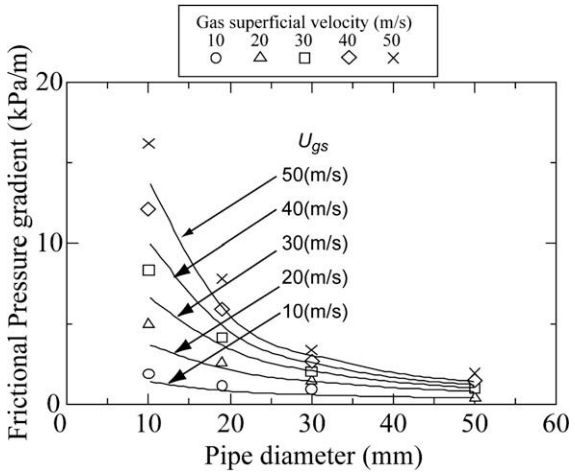

Fig. 15. Effect of pipe diameter on frictional pressure gradient (liquid superficial velocity = 0.1 m/s).

curve for lower mixture velocity. It is found that the deviation from this curve increases systematically with pipe diameter, as indicated by the arrows. It has been proposed by Sawai et al. (2004) and Kaji et al. (2007) that the deviation from Nicklin et al. curve represents the transition from slug to churn flow. The evidence shows that the transition to churn flow shifts to higher gas flow rates as the pipe diameter increases.

In considering the parametric dependence of the structure velocities, it has been seen that this parameter shows trends similar to those shown in Figs. 9 and 16 when plotted against void fraction, or homogeneous void fraction, i.e., there is a maximum and a minimum in the data. In considering dimensionless groups, it can be seen that some insight can be gained from non-dimensionalising the structure velocity by the gas superficial velocity and plotting it against the Froude number, = $u_{gs}\sqrt{\rho_g}\Big/\sqrt{([\rho_l-\rho_g]gD_t)}$. This group is sometimes termed u_g^*. Again there is little effect of pipe diameter seen in Fig. 17 for lower values of Froude number but there is still a pipe diameter effect at higher

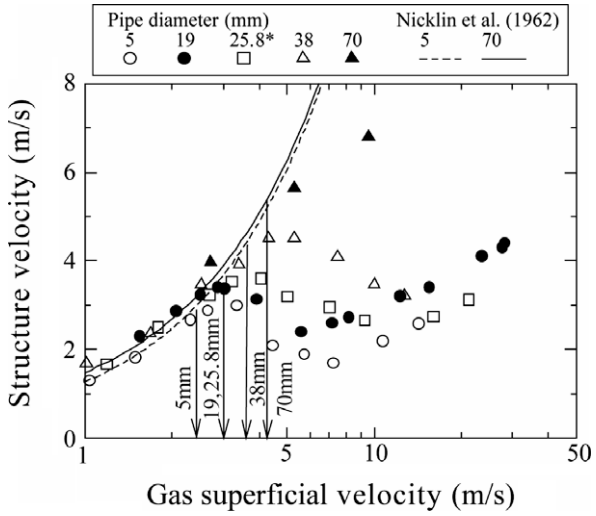

Fig. 16. Deviating points from the curve of Nicklin et al. (1962) for different pipe diameters at a constant liquid flow rate. The arrows indicate the conditions at which the deviation from the Nicklin et al. curves (liquid superficial velocity = 0.25 m/s).

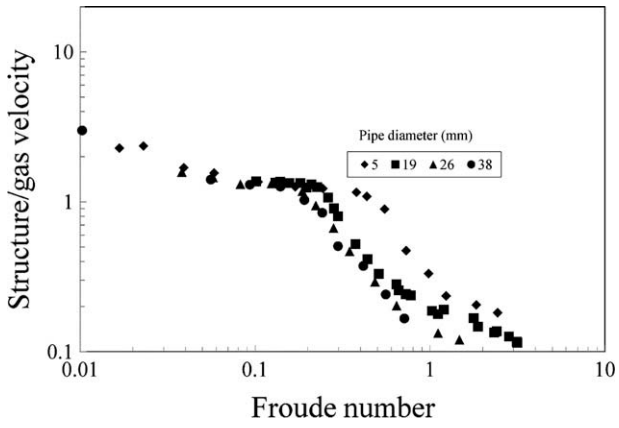

Fig. 17. Relationship between dimensionless structure velocity and Froude number.

Froude numbers. The insensitivity to pipe diameter in the slug flow region (which corresponds to lower Froude numbers is reflected in the good agreement with the equation proposed by Nicklin et al. (1962) and illustrated in Figs. 9 and 16. At higher Froude numbers, annular flow, the data has other dependencies as demonstrated below when comparison is made with the disturbance wave model of Pearce (1979).

5.5. Disturbance waves in annular flow

The data on the velocities of disturbance waves have been obtained from the cross correlation of the entire time series of void fraction, the results will include the velocities of huge waves if they are present as well as those of disturbance waves. To minimise the effects of huge waves only data from greater than 10 m/s gas superficial velocity were considered where those waves are unlikely. The results (Cases 1–13 and 19) plotted against mixture velocity for different pipe diameters at a constant liquid flow rate are shown in Figs. 18a–d. Similar results from some pipe diameters can be found from low and high gas flow rates. The pipe diameter classified into eight groups, i.e., 5, 10, 19, 25, 29, 32, 42 and 50 mm. The 6 mm data from Ide et al., the 9.5 mm data from Jong and Gabriel, and the 25.8 mm data from Sekoguchi et al./Sekoguchi and Mori were categorised as 5 mm, 10 mm and 25 mm, respectively. From the figure, at a liquid superficial velocity of 0.03 m/s the effect of pipe diameter on disturbance waves is minor but the wave velocity becomes widely distributed as liquid superficial velocity increases. Fig. 19 shows the structure velocity from different pipe diameters at a constant liquid superficial velocity of 0.1 m/s together with the data from Ide et al. (1993). The figure shows that the velocity of disturbance waves decreases systematically with pipe diameter.

Omebere-Iyari and Azzopardi (2007) assessed the effect of pipe diameter on the model of Pearce (1979). They analysed data from the whole range of liquid superficial velocity and reported that Pearce coefficient, K, increased with increasing pipe diameter. However, as shown in Fig. 15 the wave velocity also depends on the liquid superficial velocity. Therefore, the effect of pipe diameter needs to be assessed at each fixed liquid superficial velocity. The correlation of Pearce has been applied to the smallest and largest diameter pipes at each liquid flow rates and values of K are extracted and plotted in Fig. 20. From the figure, it is seen that the variation in the Pearce coefficient between small and large diameter pipes becomes larger with increasing liquid flow rates. For some data from large diameter pipes at the higher liquid flow rate it found to be above 1. This is unrealistic and probably because of

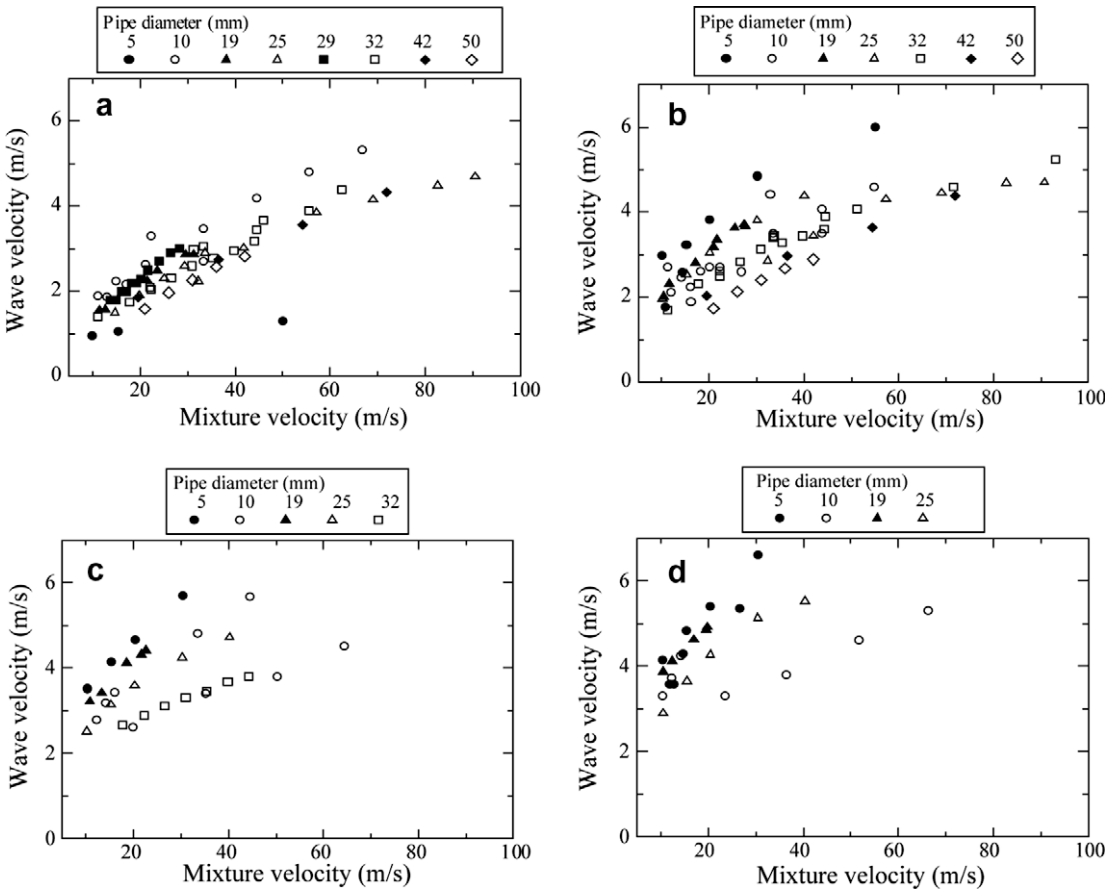

Fig. 18. Effect of pipe diameter on velocity of disturbance waves at different liquid flow rates. ((a–d) corresponds to liquid superficial velocities of 0.03, 0.1, 0.2 and 0.4 m/s, respectively).

the underestimation of liquid film velocities. As reported by Omebere-Iyari and Azzopardi (2007), K increases with increasing pipe diameter. They considered that the reason of the difference is the decrease in coherence of wave structure around the circumference in larger diameter pipes. The thickness at the peak of the wave, δ_p, is greater when the structure is coherent, whilst the difference of base and average film thickness, δ_b and $\bar{\delta}$, can be negligible. From the definition of the Pearce coefficient (Eq. (19)), K increases with increasing pipe diameter.

In the case where the liquid flow rate increases at small pipe diameter, similar interpretation is possible. In this case, δ_p might become bigger with increasing the liquid flow rate. For larger pipe, the incoherence of the structure can be an important effect. However, the link is not totally clear. The finding from Fig. 20 is that Peace coefficient is not a true constant as the liquid flow rate increases. Pearce (1979) suggested a value of K of 0.8 from the test using 31.8 mm pipe diameter. This is a reasonable initial value but it needs to be improved.

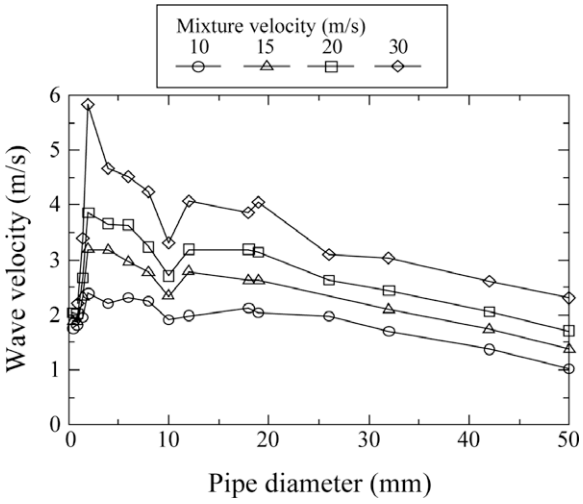

Fig. 19. Effect of pipe diameter on velocity of disturbance waves combining with the results from Ide et al. (1993) at a constant liquid superficial velocity of 0.1 m/s.

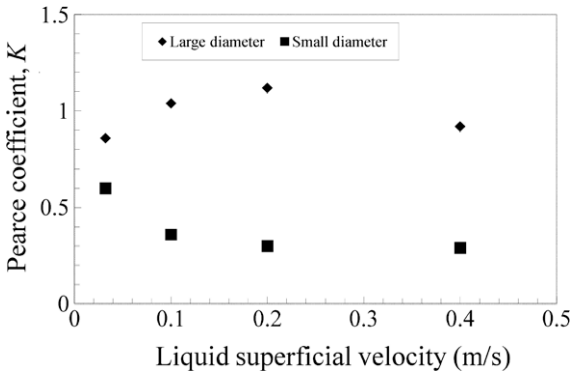

Fig. 20. Variation of Pearce coefficient with liquid flow rate for different pipe diameters.

6. Conclusions

Time series of cross-sectional average void fraction were obtained by ring-type conductance probes mounted on a 19 mm pipe. The velocity of periodic structure was derived by cross correlation using information of two successive probes. The pressure gradient was also obtained simultaneously. Using these experimental results and a published data bank from 5 to 50 mm pipes at dimensionless axial distance >100 pipe diameters, i.e., considered as a fully developed flow, the effect of pipe diameter on flow characteristics was investigated. Validation of empirical models was also provided.

Following conclusions can be drawn:

1. Average film thickness and the gas flow rate where slug/churn and churn/annular transitions occur increase with pipe diameter. On the other hand, pressure gradient, frequencies and velocities of the periodic structures decrease.
2. The correlations of Asali et al. (1985) and Kosky (1971) for film thickness and Ambrosini et al. (1991) for frictional pressure gradient have been tested against the data from the different pipe diameters. The correlations underestimates at larger pipe diameters for film thickness and at smaller pipe diameters for frictional pressure gradient. It is verified that these correlations performs best for 20–30 mm pipes.
3. The velocity of disturbance waves is widely distributed for higher liquid flow rates. The coefficient proposed by Pearce in his model $K = 0.8$ is reasonable for lower liquid flow rates but there is a room to improve especially for higher liquid flow rates.

Acknowledgements

This work has been undertaken within the Joint Project on Transient Multiphase Flow (TMF3). The author(s) wish to acknowledge the contributions made to this project by the Engineering and Physical Science Research Council (EPSRC), the Department of Trade and Industry and the following:- Advantica; AspenTech; BP Exploration; Chevron; ConocoPhillips; ENI; ExxonMobil; FEESA; Granherne/Subsea 7; Institutt for Energireknikk; Institut Français du Petrole; Norsk Hydro; Petrobas, Scandpower; Shell; Statoil and TOTAL. The authors wish to express their sincere gratitude for this support.

References

Ambrosini, W., Andreussi, P., Azzopardi, B.J., 1991. A physically based correlation for drop size in annular flow. Int. J. Multiphase Flow 17 (4), 497–507.
Asali, J.C., Hanratty, T.J., Andreussi, P., 1985. Interfacial drag and film height for vertical annular flow. AIChE J. 31 (6), 895–902.
Azzopardi, B.J., 1986. Disturbance wave frequencies, velocities and spacing in vertical annular two-phase flow. Nucl. Eng. Des. 92, 121–133.
Belt, R.J., Van't Westende, J.M.C., Portela, L.M., 2009. Prediction of the interfacial shear-stress in vertical annular flow. Int. J. Multiphase Flow 35, 689–697.
Fossa, M., 1998. Design and performance of a conductance probe for measuring the liquid fraction in two-phase gas–liquid flows. Flow Measure. Instrum. 9, 103–109.
Hernandez Perez, V., Azzopardi, B.J., 2006. Effect of inclination on gas–liquid flows. In: 10th International Conference on Multiphase Flow in Industrial Plant, Tropea (VV), Italy, 20–22 September.
Hewitt, G.F., Govan, A.H., 1990. Phenomenological modelling of non-equilibrium flows with phase change. Int. J. Heat Mass Transf. 33 (2), 229–242.
Holt, A.J., 1996. Pressure drop and void fraction in narrow channels. Ph.D. Thesis, The University of Nottingham, Nottingham, UK.
Holt, A.J., Azzopardi, B.J., Biddulph, M.W., 1999. Calculation of two-phase pressure drop for vertical upflow in narrow passages by means of a flow pattern specific model. Trans. Inst. Chem. Eng. 77, 7–15.
Ide, H., Matsumura, H., Kado, H., 1993. Velocity of liquid lumps in vertical upward gas–liquid two-phase flow in capillary tubes (effect of tube diameter in annular flow. Trans. JSME Series B 59, 795–801.
Jayanti, S., Tokarz, A., Hewitt, G.F., 1996. Theoretical investigation of the diameter effect on flooding in countercurrent flow. Int. J. Multiphase Flow 22 (2), 307–324.
Jong, P., Gabriel, K.S., 2003. A preliminary study of two-phase annular flow at microgravity: experimental data of film thickness. Int. J. Multiphase Flow 29, 1203–1220.
Kaji, R., 2008. Characteristics of two-phase structures and transitions in vertical upflow. Ph.D. Thesis, University of Nottingham.
Kaji, R., Azzopardi, B.J., Lucas, D., 2009. Investigation of flow development of co-currentgas-liquid vertical slug flow. Int. J. Multiphase Flow 35, 335–348.
Kaji, R., Omebere-Iyari, N.K., Hernandez Perez, V., Azzopardi, B.J., 2007. The effect of pipe diameter on flow patterns in vertical upflow. In: 6th International Conference on Multiphase Flow, Leipzig, 9–13 July.
Kosky, P.G., 1971. Thin liquid films under simultaneous shear sand gravity forces. Int. J. Heat Mass Transf. 14, 1220–1224.
Martin, C.J., 1983. Annular two-phase flow. D.Phil. Thesis, University of Oxford, UK.
Nicklin, D.J., Wilkes, J.O., Davidson, J.F., 1962. Two-phase flow in vertical tubes. Trans. Inst. Chem. Eng. 40, 61–68.
Ohba, K., Nagae, K., 1993. Characteristics and behaviour of the interfacial wave on the liquid film in a vertical upward air–water two-phase annular flow. Nucl. Eng. Des. 141, 17–25.
Ohnuki, A., Akimoto, H., 2000. Experimental study on transition of flow pattern and phase distribution in upward air–water two-phase flow along a large vertical pipe. Int. J. Multiphase Flow 26, 367–386.
Omebere-Iyari, N.K., 2006. The effect of pipe diameter and pressure in vertical two-phase flow. Ph.D. Thesis, The University of Nottingham, UK.
Omebere-Iyari, N.K., Azzopardi, B.J., 2007. A study of flow patterns for gas/liquid flow in small diameter tubes. Chem. Eng. Res. Des. 85 (A2), 1–13.
Pearce, D.L., 1979. Film waves in horizontal annular flow: space-time correlator experiments. Central Electricity Research Laboratories, Report RD/L/N/111/79.
Sawai, T., Kaji, M., Kasugai, T., Nakashima, H., Mori, T., 2004. Gas–liquid interfacial structure and pressure drop characteristics of churn flow. Exp. Therm. Fluid Sci. 28, 597–606.
Schadel, S.A., 1988. Atomization and deposition rates in vertical annular two-phase flow. Ph.D. Thesis, University of Illinois, USA.
Sekoguchi, K., Mori, K., 1997. New development of experimental study on interfacial structure in gas–liquid two-phase flow. In: Giot, M., Mayinger, F., Celata, G.-P. (Eds.), Experimental Heat Transfer, Fluid Mechanics and Thermodynamics. Edizione ETS 2, pp. 1177–1188.
Sekoguchi, K., Nishikawa, K., Nakasatomi, M., Nishi, H., Kaneugi, A., 1973. Liquid film flow phenomena in upwards two-phase annular flow. Trans. JSME 39, 313–323.
Sekoguchi, K., Ueno, T., Tanaka, O., 1985. An investigation of the flow characteristics in the disturbance wave region of annular flow: 2nd report, on correlation of principal flow parameters. Trans. JSME Series B 51, 1798–1806.
Sekoguchi, K., Ide, H., Matsumura, H., Takeishi, M., Kado, H., Nakasatomi, M., 1992. Velocity of liquid lumps in vertical upward gas–liquid two-phase flow in capillary tubes. Trans. JSME Series B 58, 1372–1377.
Tomida, T., Okazaki, T., 1974. Statistical character of large disturbance waves in upward two-phase flow of air–water mixtures. J. Chem. Eng. Jpn 7, 329–333.
Tsochatzidis, N.A., Karapantsios, T.D., Vostoglou, M.V., Karabelas, A.J., 1992. A conductance probe for measuring liquid fraction in pipes and packed beds. Int. J. Multiphase Flow 18 (5), 653–667.
Vijayan, M., Jayanti, S., Balakrishnan, A.R., 2001. Effect of tube diameter on flooding. Int. J. Multiphase Flow 27 (5), 797–816.
Willets, I.P., 1987. Non-aqueous annular two-phase flow. D.Phil. Thesis, University of Oxford, UK.
Wolf, A., Jayanti, S., Hewitt, G.F., 2001. Flow development in vertical annular flow. Chem. Eng. Sci. 56, 3221–3235.